Received: 1 May 2023 | Revised: 16 November 2023 | Accepted: 3 January 2024

DOI: 10.1002/hbm.26595

RESEARCH ARTICLE

WILEY

# Deep learning-based BMI inference from structural brain MRI reflects brain alterations following lifestyle intervention

Ofek Finkelstein[1] | Gidon Levakov[1] | Alon Kaplan[2,3] | Hila Zelicha[2] | Anat Yaskolka Meir[2] | Ehud Rinott[2] | Gal Tsaban[2,4] | Anja Veronica Witte[5] | Matthias Blüher[6] | Michael Stumvoll[6] | Ilan Shelef[2,4] | Iris Shai[2,7] | Tammy Riklin Raviv[8] | Galia Avidan[9]

[1]Department of Cognitive and Brain Sciences, Ben-Gurion University of the Negev, Beer Sheva, Israel

[2]The Health & Nutrition Innovative International Research Center, Faculty of Health Sciences, Ben Gurion University of the Negev, Beer Sheva, Israel

[3]The Chaim Sheba Medical Center, Tel Hashomer, Ramat-Gan, Israel

[4]Soroka University Medical Center, Beer Sheva, Israel

[5]Department of Neurology, Max Planck-Institute for Human Cognitive and Brain Sciences, and Cognitive Neurology, University of Leipzig Medical Center, Leipzig, Germany

[6]Department of Medicine, University of Leipzig, Leipzig, Germany

[7]Department of Nutrition, Harvard T.H. Chan School of Public Health, Boston, Massachusetts, USA

[8]The School of Electrical and Computer Engineering, Ben Gurion University of the Negev, Beer Sheva, Israel

[9]Department of Psychology, Ben-Gurion University of the Negev, Beer Sheva, Israel

**Correspondence**
Ofek Finkelstein, Department of Cognitive and Brain Sciences, Ben-Gurion University of the Negev, Beer Sheva, Israel.
Email: ofekfink@post.bgu.ac.il

Tammy Riklin Raviv, The School of Electrical and Computer Engineering, Ben Gurion University of the Negev, Beer Sheva, Israel.
Email: rrtammy@bgu.ac.il

Galia Avidan, Department of Psychology, Ben-Gurion University of the Negev, Beer Sheva, Israel.
Email: galiaa@bgu.ac.il

**Funding information**
National Institutes of Health, Grant/Award Number: U01 AG024904; Department of Defense, Grant/Award Number: W81XWH-12-2-0012; NIMH, Grant/Award Numbers: 5R21MH107045, R03MH096321, K23MH087770; UK Biotechnology and Biological Sciences Research Council, Grant/Award Number: BB/H008217/1; German Research Foundation, Grant/Award

## Abstract

Obesity is associated with negative effects on the brain. We exploit Artificial Intelligence (AI) tools to explore whether differences in clinical measurements following lifestyle interventions in overweight population could be reflected in brain morphology. In the DIRECT-PLUS clinical trial, participants with criterion for metabolic syndrome underwent an 18-month lifestyle intervention. Structural brain MRIs were acquired before and after the intervention. We utilized an ensemble learning framework to predict Body-Mass Index (BMI) scores, which correspond to adiposity-related clinical measurements from brain MRIs. We revealed that patient-specific reduction in BMI predictions was associated with actual weight loss and was significantly higher in active diet groups compared to a control group. Moreover, explainable AI (XAI) maps highlighted brain regions contributing to BMI predictions that were distinct from regions associated with age prediction. Our DIRECT-PLUS analysis results imply that predicted BMI and its reduction are unique neural biomarkers for obesity-related brain modifications and weight loss.

Ofek Finkelstein and Gidon Levakov share first authorship. Tammy Riklin Raviv and Galia Avidan share last authorship.

Number: 209933838-SFB 1052; Israel Ministry of Health, Grant/Award Number: 87472511; Israel Ministry of Science and Technology, Grant/Award Number: 3-13604

KEYWORDS
biomarker, deep learning, MRI, obesity

## 1 | INTRODUCTION

Obesity is an epidemic-scale disease associated with multiple comorbidities, such as diabetes (Leong & Wilding, 1999), liver disease (Scheen & Luyckx, 2002) and dementia (Alford et al., 2018; Kivipelto et al., 2005; Razay et al., 2006; Whitmer et al., 2005). The negative impact of obesity on the brain (Uranga & Keller, 2019) includes reduced gray matter volume (Han et al., 2021; Pannacciulli et al., 2006), increase in inflammation markers and cognitive decline (Nguyen et al., 2014; Spyridaki et al., 2016). Evidence suggests that lifestyle intervention may attenuate some of the neural changes associated with obesity (Kaplan et al., 2022). However, assessing these beneficial neural outcomes is challenging as the effect of obesity on the brain is complex and multifaceted (Shefer et al., 2013; Uranga & Keller, 2019).

Lifestyle interventions were shown to have a positive impact on general health, initiating changes such as weight loss, revised liver status, and improved vascular health. Some interventions were beneficial also at the cognitive and neural levels, eliciting changes in cognitive performance (Arjmand et al., 2022), brain morphometry (Espeland et al., 2016; Kaplan et al., 2022), and functional connectivity (Levakov et al., 2023).

Deep learning frameworks have led to significant advancements in a variety of fields including Computational Neuroscience. In recent studies, deep neural networks (DNNs) were exploited to predict the "brain age" of healthy subjects from structural brain MRI. These networks were trained on paired datasets which included MRI scans and subjects' chronological age. Once trained, at the inference phase, the networks can predict brain age based only on the imaging data, which can be either structural as done in the current study (Cole et al., 2017; Franke et al., 2012) or functional (Levakov et al., 2023; Lund et al., 2022). The predicted age may differ from one's chronological age. The discrepancy between chronological and brain age is an established biomarker, associated with neurodegenerative diseases (Bocancea et al., 2021) as well as higher mortality rates (Cole et al., 2018).

The scientific potential and clinical significance of brain-age biomarkers inspired related studies, aiming to associate particular physical traits to brain morphology. Nevertheless, to investigate such associations, the DNN-based prediction model should be trained on large brain MRI datasets that include the respective subjects' traits. One such trait is the Body Mass Index (BMI) which is often available in public brain MRI datasets. BMI is a simple, widely used measure for assessing obesity, while taking height into consideration. Previous studies showed that BMI could be estimated from structural MRI using convolutional DNNs (Vakli et al., 2020; Yadav & Razavian, 2019). In this work, we adapted a similar strategy to explore whether differences in clinical measurements following lifestyle intervention in an overweight population could be reflected in the brain. Specifically, we aimed to address the following questions: (1) Can a deep learning-based BMI prediction framework, fitted on a normal population, be applied to a separate, overweight population? (2) If so, to what extent would such predictions be correlated with other health biomarkers? (3) Would weight loss related changes that occurred following lifestyle intervention be reflected in the predicted BMI? and (4) To what extent would the features used to predict BMI be distinct from those used in predicting age?

Our model was trained, validated, and tested on a sample of 19,275 brain images. The fitted model was then applied to 216 participants from the DIRECT-PLUS study (Dietary Intervention Randomized Controlled Trial Polyphenols Unprocessed Study, Yaskolka Meir et al., 2021). The DIRECT-PLUS study was an 18-month-long clinical trial. Participants who passed the criterion for metabolic syndrome (abdominal obesity/dyslipidemia) were randomly divided into three diet groups: healthy dietary guidelines (HDG, an active control group), Mediterranean diet (MED), and green-MED. All participants underwent a T1 brain MRI scan at baseline and 18 months after the intervention. In addition, all were assessed before and after the intervention for multiple clinical measurements, including anthropometry, liver and glycemic markers, lipid profile, and fat deposition. Since neither of these relevant clinical measures was available in the brain MRI datasets we used for DNN training, we chose to predict BMI as their proxy (see Figure 1). Although BMI is a measure of obesity and does not qualify as a criterion for a metabolic syndrome, it was shown to be correlated with waist circumference in patients with metabolic syndrome (Gierach et al., 2014; Weiss et al., 2004). In addition, we generated explainable AI maps to detect brain regions that contributed to the prediction.

## 2 | MATERIALS AND METHODS

### 2.1 | Participants

#### 2.1.1 | Dataset used for training and validating

To train a model that could handle large variability associated with subjects' demography and scan-related differences, we collated training data from eight different open datasets. We only included samples with available BMI, age, gender, and a T1w MRI brain scan. Subjects with diagnosed neurological conditions were excluded. The total sample size was 19,275, randomly divided into training ($N = 13{,}471$; 70%), validation ($N = 1957$; 10%) and testing ($N = 3847$; 20%). See Table S1 in Supplementary section 1 for a list of the studies and corresponding BMI, age, and gender distributions.

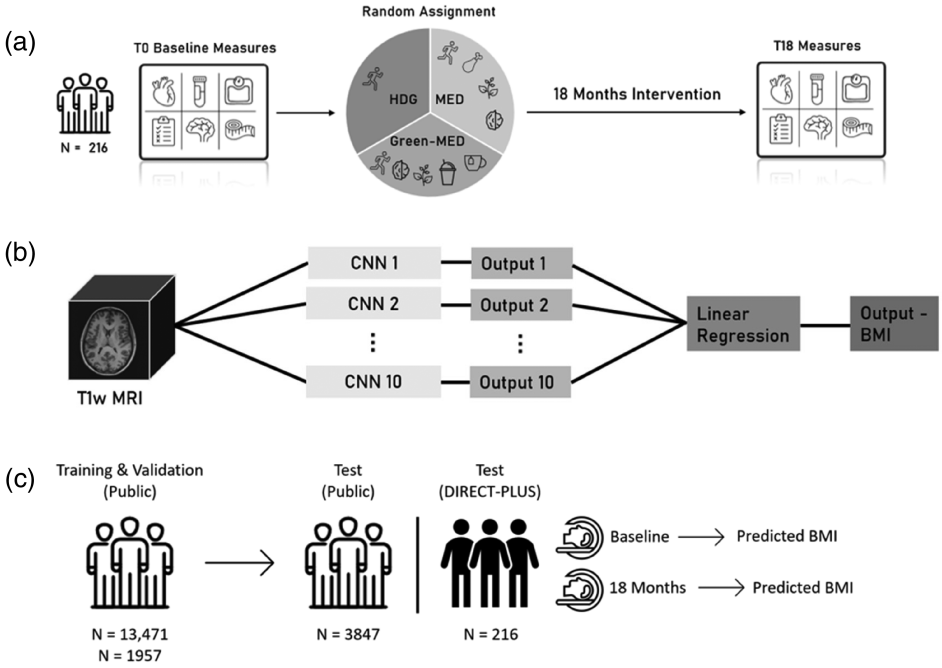


**FIGURE 1** Study design and analysis overview. (a) The DIRECT-PLUS was an 18-months lifestyle intervention clinical trial. Participants were randomly assigned to one of three intervention groups: healthy dietary guidelines (HDG) which served as an active control group, Mediterranean diet (MED), and green-MED. All intervention groups were combined with physical activity (PA) and participants were assessed before and after the intervention (T0 and T18 correspondingly). Assessments included anthropometric measurements, blood biomarkers, fat deposition, and brain imaging. For more details, see Section 2.1.2. (b) The suggested ensemble architecture consisted of 10 CNN regressors ensembled by linear regression to a single scalar representing BMI. Then, saliency maps were extracted based on the predictions to reveal contributing brain regions. (c) Sub-study design. The suggested model was trained and validated on a collation of public datasets to predict BMI, and later tested on an independent test set as well as on the DIRECT-PLUS dataset at T0 and T18.

### 2.1.2 | The DIRECT-PLUS study

*Study description*

This work was based on a sub-study of the DIREC-PLUS clinical trial (clinicaltrials.gov ID: NCT03020186). The Dietary Intervention RandomizEd Controlled Trial PoLyphenols UnproceSsed (DIRECT-PLUS, Yaskolka Meir et al., 2021) trial was initiated in 2017 and lasted 18 months. During the trial, a group of participants who fitted the criterion for metabolic syndrome (abdominal obesity or dyslipidemia) underwent a lifestyle intervention. Participants were scanned (structural MRI) and multiple clinical measures were taken at baseline and 18 months following the beginning of the trial. We refer to data from baseline as T0 and data from the end of the trial, 18 months later as T18. Out of 378 volunteers, 294 met the inclusion criteria of age (30+) and abdominal obesity or dyslipidemia, where 89% had abdominal obesity. Abdominal obesity was measured by waist circumference (WC, men >102 cm, and women >88 cm), while dyslipidemia by Triglycerides (TG > 150 mg/dl) and high-density lipoprotein cholesterol (HDL-c, men ≤40 mg/dl and women ≤50 mg/dl). The 216 participants who completed the two structural brain scans at T0 and T18 were included in this sub-trial. The Soroka Medical Center Medical Ethics Board and Institutional Review Board provided ethics approval. All participants provided written consent and received no financial compensation.

*Randomization and intervention*

Participants were randomly divided into one of three weight-loss diet groups, Healthy Dietary Guidelines (HDG), Mediterranean Diet (MED), and green-MED, all accompanied by physical activity. All participants received free gym membership and dietary guidance and consultation and were aware of their assigned diet group (open-label protocol).

*MRI acquisition*

MRI scans were conducted at the Soroka University Medical Center (SUMC), Beer Sheva. Participants were scanned in a 3 T Philips Ingenia scanner (Amsterdam, The Netherlands) equipped with a standard head coil. Subjects were instructed to refrain from food and non-water beverages 2 h before the MRI sessions. Each of the two sessions before and after the intervention included a 3D T1-weighted anatomical scan. High-resolution anatomical volumes were acquired with a T1-weighted 3D pulse sequence ($1 \times 1 \times 1\ mm^3$, 150 slices, TR = 2500, TE = 30 ms, field of view $240 \times 220 \times 150$). Details regarding the abdominal and liver fat deposition acquisition are available in Data S1, section 8: Liver and visceral fat imaging protocols.

*BMI and additional clinical measurements*

All measures were taken for each participant at baseline (T0) and after 18 months of intervention (T18). BMI was calculated by dividing

participants' weight (in kg) by squared height (in m), hence measured by units of $\frac{kg}{m^2}$. Bodyweight was measured without shoes to the nearest 0.1 kg, and height was measured to the nearest millimeter using a standard wall-mounted stadiometer. Waist circumference was measured to the nearest millimeter using an anthropometric measuring tape, halfway between the last rib and the iliac crest. Serum total cholesterol (TC) and High-density lipoprotein cholesterol (HDL-c) were determined enzymatically. Plasma glucose and insulin levels, and Plasma polyphenols metabolites were also measured. An assessment of nutritional intake and lifestyle habits was self-reported by a computer-administered questionnaire. Additional measures, such as blood samples, fecal samples, and intrahepatic fat (IHF) were taken as well.

## 2.2 | Preprocessing

We applied the following preprocessing steps to the T1w images using Nipype (Gorgolewski et al., 2011). First, the neck and shoulders were removed from each scan using RobustFov (Jenkinson et al., 2012). Next, brain extraction was performed using Robex (Iglesias et al., 2011), followed by an expansion of the brain mask to include the CSF surrounding the brain. The image was then corrected for intensity non-uniformity with N4BiasFieldCorrection (Tustison et al., 2010). Next, intensity normalization was applied using fuzzy c-means, and WM-based mean normalization (Reinhold et al., 2018). Finally, images were resampled to a $1.75 \times 1.75 \times 1.75$ $mm^3$ isotropic resolution and cropped to a $90 \times 120 \times 99$ voxels box around the center of mass of the brain mask.

## 2.3 | BMI and age estimation

To estimate age and BMI we utilized an ensemble architecture, previously developed in our lab (Levakov et al., 2020). We trained two different ensembles for BMI and age, respectively. Each ensemble was composed of 10 CNN models, randomly initialized, and separately trained to predict age or BMI. For additional details of a single CNN architecture, see Section 2.7. The loss function of each CNN was defined as the MSE (mean squared error) between observed and predicted BMI or age. Finally, to optimally combine the 10 outputs to a single output scalar, we used a linear regression model. See Figure 1b for the architecture of the entire model. For training and validation, we used the open dataset's training and validation sets, described in Section 2.1.1. For testing, we used a separate test set from the open datasets, as well as the DIRECT-PLUS dataset at T0 and T18. We trained each CNN for 50 epochs using the Adam optimizer (lr = 0.00015). The linear regression model was trained on the validation set of the open dataset. The overall model's accuracy was evaluated using mean absolute error (MAE) and Pearson correlation coefficient between the network predictions and observed BMI or age. Code and weights are available at: https://github.com/ofekfink/BMI_Prediction.git.

## 2.4 | Models' explainability and features similarity

We created ensemble population-based explanation maps to reveal brain regions that contributed to the models' predictions. The maps were based on each of the trained ensembles separately (BMI/age), and on an additional ensemble of five random untrained CNNs as a control (Adebayo et al., 2018). Population-based maps were previously shown to be more consistent and reliable across groups of subjects (Levakov et al., 2020). To generate such maps, we followed a previously developed methodology that introduced an inference scheme, which enables averaging the individual maps to population-based ones (Levakov et al., 2020). Then, from the thresholded maps (first percentile), we extracted clusters bigger than 100 voxels, and identified the corresponding brain regions. To validate that the brain regions highlighted by the explanation maps were relevant and specific to the predicted domain, we compared the BMI and age based maps. We created these maps for 100 random subjects from the DIRECT-PLUS dataset, at T0 and T18. To quantify the differences between types of explanation maps, we compared each pair of maps before aggregating over different CNNs ($N = 25$, 10 for age prediction, 10 for BMI prediction, and five random untrained for sanity check) using the Dice similarity coefficient: Let X and Y be two sets of voxels that passed the threshold in two different XAI maps. The Dice score is calculated according to the following formula: $\frac{2|X \cap Y|}{|X|+|Y|}$ (Dice, 1945), where $|X|$, $|Y|$ are the number of voxels in each set, and $|X \cap Y|$ is the number of intersecting voxels. See Section 2.7 for additional elaboration.

## 2.5 | Statistical analysis

In all relevant analyses, we accounted for multiple comparisons using False Discovery Rate (FDR, Benjamini & Hochberg, 1995). Student's t-test (Student, 1908) was used to compare between the predicted BMI loss of the control group (HDG) and the active intervention groups (Med and Green-Med), as well as to compare between the Dice scores of different explanation maps. To control for the effect of the observed BMI on the BMI predictions, a linear regression model was used to predict the desired clinical outcome with the observed BMI or age covariates as predictors, keeping only the residual. To correct for regression attenuation bias when predicting BMI at each time point (T0 and T18), we used a correction methodology previously described for age prediction (Beheshti et al., 2019). An offset was subtracted from the BMI predictions. This offset was calculated as $\text{offset} = s * \text{observed BMI} + i$, where s and i are the slope and the intercept of a linear least-squares regression model of predicted BMI minus observed BMI against observed BMI. The bias of predicted BMI loss is calculated as T0 corrected minus T18 corrected. This correction procedure was used only during inference and not for testing the correlation between the predicted and observed BMI. When testing for significant differences of the predicted BMI loss between the intervention groups, outliers were defined as subjects whose

predicted loss after bias correction was 2 or more standard deviations away from the mean predicted loss after bias correction.

## 2.6 | Implementation details

CNN models were implemented using Keras (Chollet et al., 2018). Each CNN model received a 3D volume of size 90 × 120 × 99 as input, and its output was a single scalar representing BMI or chronological age. Each CNN model was comprised of three blocks, each containing two 3D convolution layers (3 × 3 × 3 filters), followed by max-pooling and batch normalization layers. Those blocks were then followed by a dropout layer and two fully connected layers. Each layer included a rectified linear unit (ReLU) activation function. For a detailed description of the architecture, see Figure S1 in Data S1 section 3.

To generate population-based explanation maps, we followed the aforementioned inference scheme (Levakov et al., 2020): first, a subject-specific explanation map was generated for 100 random subjects from the DIRECT-PLUS dataset, using the SmoothGrad algorithm (Smilkov et al., 2017) implemented as iNNvestigate (Alber et al., 2018). The SmoothGrad method adds random noise from a normal distribution to an input image and then computes the partial derivative of each voxel with respect to the trained model's output. We repeated this process 64 times and averaged the results. Then, each map was registered to the subject's anatomical image and aligned to MNI space using FreeSurfer (Fischl, 2012). Next, each volume was standardized and smoothed with a 3D Gaussian (van der Walt et al., 2014) and averaged across subjects. Finally, to aggregate the CNNs maps of each ensemble, each voxel's median was calculated and taken across the generated maps.

Then, using FSL cluster (Woolrich et al., 2009) we extracted clusters of voxels from the thresholded explanation maps (first percentile) and focused on clusters bigger than 100 voxels. Due to FSL's clustering algorithm, which creates spatially close clusters, a cluster could contain voxels from multiple anatomical brain regions. To identify the analogous brain regions, we used each cluster's MNI coordinates at the point of maximum intensity. To match the aforementioned coordinates to brain regions, we used the following atlases: Desikan–Killiany Atlas for GM structures (Desikan et al., 2006), ICBM-DTI-81 white-matter labels atlas for WM structures (Mori et al., 2006), and manually for CSF spaces.

# 3 | RESULTS

We first demonstrated that in a held-out sample, the predicted BMI was significantly correlated with the observed BMI. We then showed that the predicted BMI was associated with multiple clinical outcomes after controlling for the observed BMI. Next, we verified that weight loss and characteristics of the lifestyle intervention (e.g., specific diet) were reflected in the predictions. Lastly, we revealed that brain regions contributing the most to BMI predictions were distinct from age-based ROIs.

## 3.1 | BMI estimation

To estimate BMI from brain structure, we used an aggregated sample of 19,491 brain scans (mean ± SD BMI: 26.42 ± 4.51) for the model training ($n = 13{,}471$), validation ($n = 1957$), and testing ($n = 3847$). DIRECT-PLUS test set included 216 scans (mean ± SD BMI at T0: 31.02 ± 3.66, at T18: 30.12 ± 4.01). On the unseen test set, the model reached a mean absolute error (MAE) of 2.06 kg/m$^2$ and a Pearson correlation of .80 between the predicted and observed BMI ($p < .01$, Figure 2a,b). For comparison, on their test set—a subset of the UK Biobank dataset, Vakli et al. reached a MAE of 2.41 kg/m$^2$ and Pearson correlation of .7 (Vakli et al., 2020).

Applying the fitted model to the DIRECT-PLUS data at T0 resulted in a MAE of 5.29 and Pearson $r = .46$ ($p < .001$). Similar results were found at T18, with MAE = 5.23, Pearson $r = .5$ and $p < .001$ (Figure 2c,d). When tested on a subset of the unseen test set that that only includes subjects within the DIRECT-PLUS BMI range at T0 (23.73 to 50.97), the model reached a MAE of 2.11 and Pearson correlation of .69 ($p < .01$). The results of the age prediction model are available in Data S1, section 4: Age Prediction.

## 3.2 | Baseline characteristics

Baseline characteristics at T0 are described in Table 1. Note that for the following measurements: GGT, FGF21, Chemerin, Glucose, HOMA-IR, Liver Fat, VAT, SSC, and DSC, the information is incomplete for several participants.

## 3.3 | Relation between predicted BMI and clinical measurements

We asked whether the predicted BMI, based solely on brain imaging, would be correlated with obesity-related clinical measurements. We tested the correlation of predicted BMI with anthropometry, liver, glycemic, lipids, and MRI-assessed fat deposition biomarkers. We found that predicted BMI was significantly correlated ($p < .05$ after FDR correction) with BMI ($r = .456$, $p < .001$), WC ($r = .437$, $p < .001$), AST($r = .182$, $p = .007$), ALT ($r = .165$, $p = .015$), HOMA-IR ($r = .291$, $p < .001$), HDL-C ($r = -0.193$, $p = .004$), Liver Fat ($r = .322$, $p < .001$), VAT ($r = .420$, $p < .001$), and DSC ($r = .288$, $p < .001$; see Figure 3). As the observed BMI might have mediated this relation, we repeated the analysis after regressing out the observed BMI. We found that after FDR correction, HDL-C ($r = -0.188$, $p = .005$), Liver Fat ($r = .164$, $p = .02$), VAT ($r = .298$, $p < .001$), and SSC ($r = -.169$, $p = .016$) were still significantly correlated ($p < .05$) with the predicted BMI. These results imply that the predicted BMI is a neural marker related to multiple health biomarkers beyond the observed BMI. (See Figure S2a in Data S1 section 5 for a similar analysis of predicted BMI at T18).

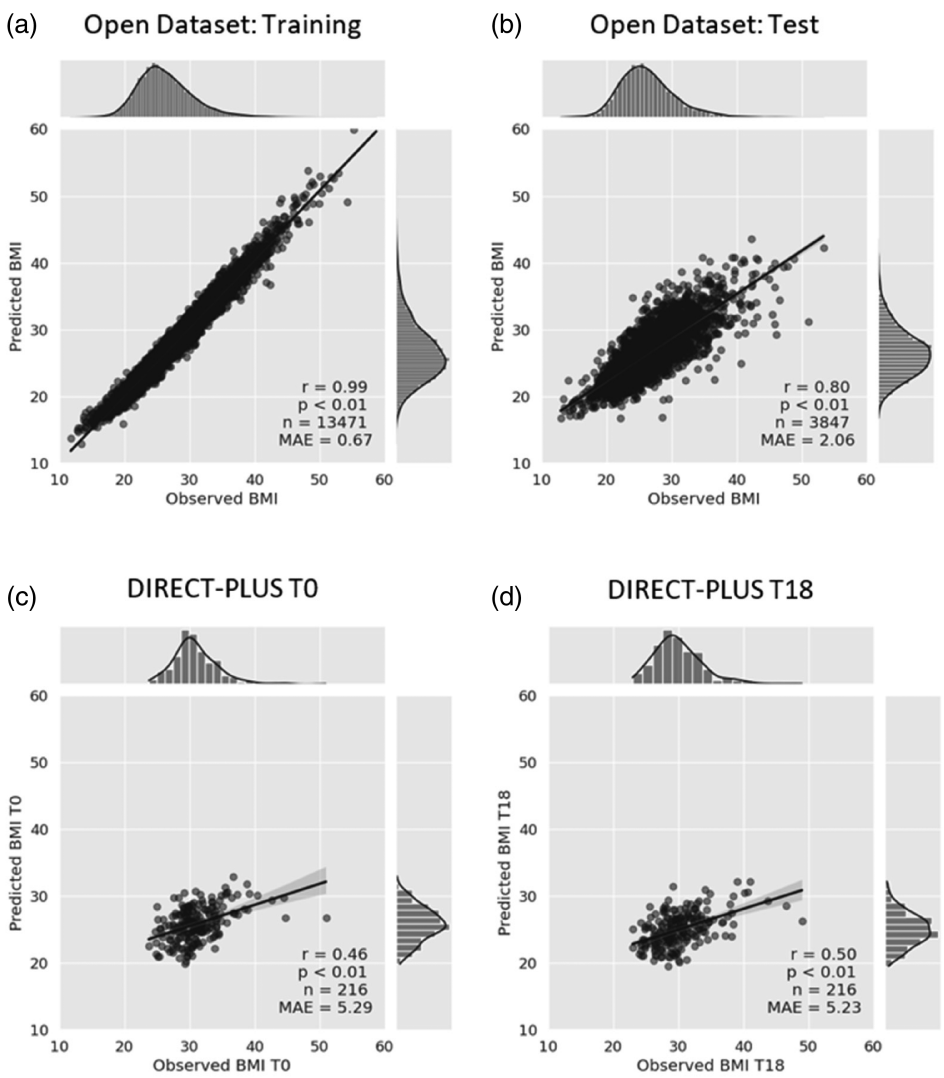


**FIGURE 2** Regression plots and histograms of observed BMI versus model's prediction for: (a) The open dataset training set (BMI mean ± SD: 26.41 ± 4.51). (b) The open dataset untouched test set (BMI mean ± SD: 26.38 ± 4.47). (c) The DIRECT-PLUS dataset at T0, overweight (BMI mean ± SD: 31.02 ± 3.66). (d) The DIRECT-PLUS dataset at T18, overweight (BMI mean ± SD: 30.12 ± 4.01). Pearson correlation coefficients between observed and predicted BMI are indicated on each plot (*r*). *p* value, the number of samples (*n*), and mean absolute error (MAE) are also noted. The model generalized from a normal to an overweight population with different BMI distribution.

### 3.4 | BMI loss prediction and group differences

As described above, predicted BMI was correlated with observed BMI. Hence, we examined whether structural brain alteration following 18 months of lifestyle intervention would be reflected in changes in the predicted BMI. We computed weight loss [before minus after the intervention] for both the predicted and the observed BMI. We found that the two weight loss values were significantly correlated ($r = .29$, $p < .001$).

Next, we asked whether a change in predicted BMI would differ among intervention groups. First, we compared all three groups (HDG, Med, and Green-MED) using one-way ANOVA. However, there were no statistically significant group differences ($F = 2.099$, $p = .125$). To further probe the potential effect of the dietary intervention, we compared the Med and Green-MED groups to the HDG, the active control group. Predicted BMI loss of the Med and Green-MED groups (1.196 ± 2.580) was significantly higher than the HDG group (0.470 ± 2.291; $t = -2.043$, $p = .042$; Figure 4b) after bias correction (Beheshti et al., 2019) and the removal of outliers (±2 STD). Taken together, these results suggest that neuronal alterations following 18 months of lifestyle intervention are reflected in the predicted BMI measure. Moreover, these changes were more pronounced following a Mediterranean diet.

### 3.5 | Models explainability and features similarity

#### 3.5.1 | Extraction of brain ROIs contributing to the model's predictions

To examine the effects of lifestyle intervention on the brain, we explored which brain regions contributed the most to the model's prediction. Voxel-wise contribution to the model's output was assessed using population-based XAI maps for each ensemble model (Section 2.4). We extracted clusters that were larger than 100 voxels from the thresholded maps (1%), and mapped them to brain regions according to their MNI coordinates. The brain regions are listed in Table 2, along with their cluster size, and MNI coordinates, where the specified coordinates are at the point of maximum intensity within the cluster. We consider the possible implications of these

**TABLE 1** Baseline characteristics of the DIRECT-PLUS at T0.

| | HDG (mean ± SD) | Med (mean ± SD) | Green-med (mean ± SD) | Test statistics (*f*, *p* values) | All (mean ± SD) | All (*n*) |
|---|---|---|---|---|---|---|
| Anthropometric measurements | | | | | | |
| Age | 51.68 ± 10.01 | 52.11 ± 10.03 | 51.21 ± 11.53 | 0.53, 0.59 | 51.66 ± 10.48 | 216 |
| Sex (% male) | 89.47% | 91.43% | 90% | 0.08, 0.92 | 90.28% | 216 |
| BMI (kg/m$^2$) | 31.16 ± 3.69 | 31.14 ± 3.9 | 30.75 ± 3.41 | 0.29, 0.75 | 31.02 ± 3.66 | 216 |
| WC (cm) | 109.12 ± 8.93 | 110.53 ± 9.62 | 108.27 ± 7.63 | 1.18, 0.31 | 109.3 ± 8.78 | 216 |
| Liver markers | | | | | | |
| AST (U/L) | 25.63 ± 7.8 | 25.86 ± 7.1 | 26.73 ± 8.38 | 0.40, 0.67 | 26.06 ± 7.75 | 216 |
| ALT (U/L) | 35.23 ± 16.39 | 34.53 ± 12.48 | 36.97 ± 18.09 | 0.44, 0.64 | 35.57 ± 15.8 | 216 |
| GGT (U/L) | 35.22 ± 26.2 | 38.12 ± 29.72 | 35.91 ± 17.95 | 0.15, 0.86 | 36.37 ± 24.81 | 202 |
| ALKP (mg/dl) | 73.67 ± 17.05 | 73.74 ± 19.71 | 75.24 ± 23.27 | 0.14, 0.87 | 74.2 ± 20.01 | 216 |
| FGF21 (pg/ml) | 183.91 ± 106.39 | 176.1 ± 101.43 | 213.22 ± 143.33 | 1.92, 0.15 | 190.77 ± 118.58 | 215 |
| Chemerin (ng/ml) | 200.64 ± 36.7 | 206.35 ± 41.16 | 203.86 ± 41.82 | 0.38, 0.69 | 203.53 ± 39.74 | 215 |
| Glycemic markers | | | | | | |
| Glucose (mg/dl) | 104.54 ± 30.04 | 100.81 ± 17.66 | 103.76 ± 21.41 | 0.49, 0.62 | 103.07 ± 23.74 | 214 |
| HOMA-IR | 3.91 ± 2.9 | 3.56 ± 1.74 | 3.56 ± 2.18 | 0.55, 0.58 | 3.68 ± 2.33 | 212 |
| HbA1c (%) | 5.53 ± 0.75 | 5.41 ± 0.47 | 5.56 ± 0.72 | 1.07, 0.34 | 5.5 ± 0.66 | 216 |
| Lipid profile | | | | | | |
| Cholesterol (mg/dl) | 190.51 ± 34.76 | 193.11 ± 27.94 | 185.03 ± 29.26 | 1.25, 0.29 | 189.58 ± 30.95 | 216 |
| HDL-C (mg/dl) | 45.71 ± 10.91 | 47.21 ± 9.03 | 47.09 ± 12.78 | 0.42, 0.66 | 46.64 ± 10.98 | 216 |
| LDL-C (mg/dl) | 125.08 ± 30.77 | 127.18 ± 28.99 | 123.86 ± 29.59 | 0.22, 0.80 | 125.36 ± 29.71 | 216 |
| Triglycerides (mg/dl) | 152.43 ± 72.74 | 149.2 ± 61.93 | 131.94 ± 58.82 | 2.05, 0.13 | 144.74 ± 65.33 | 216 |
| MRI fat deposition | | | | | | |
| Liver Fat (%) | 9.81 ± 8.16 | 9.8 ± 8.49 | 10.47 ± 9.04 | 0.13, 0.88 | 10.02 ± 8.52 | 201 |
| VAT (cm$^2$) | 127.88 ± 40.75 | 129.32 ± 47.81 | 127.55 ± 54.93 | 0.12, 0.88 | 128.22 ± 47.54 | 212 |
| SSC (cm$^2$) | 105.93 ± 39.57 | 112.89 ± 36.27 | 96.99 ± 31.59 | 0.76, 0.47 | 105.09 ± 36.27 | 203 |
| DSC (cm$^2$) | 208.47 ± 73.46 | 222.16 ± 59.89 | 202.29 ± 56.97 | 1.19, 0.31 | 210.74 ± 64.17 | 209 |

Abbreviations: Measurements: ALKP, alkaline phosphatase; ALT, alanine aminotransferase; AST, aspartate aminotransaminase; BMI, body mass index; DSC, deep subcutaneous fat; FGF21, fibroblast growth factor 21; GGT, gamma glutamyl transferase; HbA1c, hemoglobin A1c; HDL-C, high-density lipoprotein cholesterol; HOMA-IR, homoeostatic model assessment of insulin resistance; LDL-C, low-density lipoprotein cholesterol; TG, triglycerides; SSC, superficial subcutaneous fat; VAT, visceral adipose tissue; WC, waist circumference. Units: mg/dl, milligrams per decilitre; ng/ml, nanograms per millilitre; pg/ml, picogram per milliliter; U/L, units per liter.

results on the relationship between BMI and brain anatomy in the Section 4.

For XAI results obtained for a subset of subjects with high BMI in the public dataset, see Data S1, section 6: XAI Maps Results (a).

For XAI comparison between T0 and T18 in 100 subjects of the DIRECT-PLUS dataset, see Data S1, section 6: XAI Maps Results (b).

### 3.5.2 | A comparison of age and BMI XAI maps

Next, by comparing the XAI maps of age and BMI, we tested whether the two are predicted based on spatially distinct brain regions. Figure 5a,b depicts a glass brain projection of the BMI and age based ensemble models. There was only a small overlap between the two, such that the common voxels included 16.6% of the age-based map and 21.4% of the BMI-based map (Dice coefficient = 0.187). Figure 5c displays the similarity matrix comparing each pair of population-based explanation maps resulting from age, BMI, and unfitted, randomly initialized CNN models (see Section 2.4). The average Dice score between maps which resulted from the same model type was 0.369, 0.283, and 0.114 for age, BMI, and random, respectively. Contrarily, we found an average Dice score of 0.114 for all non-compatible model types. Importantly, we found that Dice scores comparing models of similar type (e.g., age and age, BMI and BMI) were higher than Dice scores comparing different types of models (e.g., age and BMI; $t = 11.663$, $p < .001$). These findings suggest that age and BMI are predicted based on distinct brain regions.

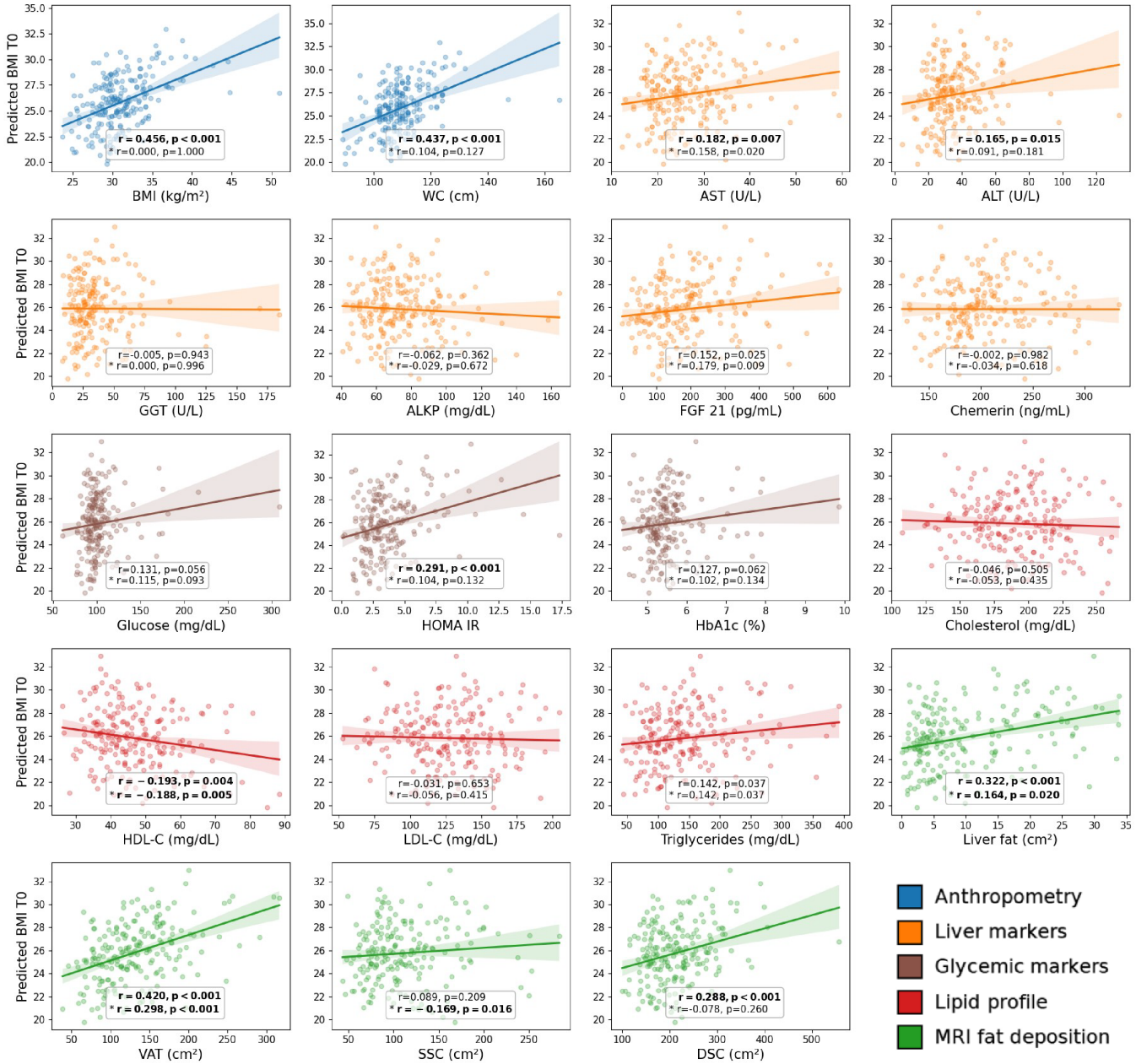


**FIGURE 3** The DIRECT-PLUS dataset ($n = 216$). Scatter plots of clinical measures taken at baseline (T0) and their association to predicted BMI at T0. Pearson's correlation coefficient between each measure to predicted BMI and the corresponding p-value are noted by *r*, *p*, while Pearson correlation coefficient between each measure to the cleaned predicted BMI (observed BMI regressed out) and the corresponding *p* value are noted by **r*, *p*. Both variations are shown at the bottom of each plot. Associations that are significant following FDR correction are marked in bold for each measure. See Section 3.2 for information about the baseline characteristics.

## 4 | DISCUSSION

In the current study, we examined the association between excessive weight and brain morphology, and how this relation changes following a lifestyle intervention. Specifically, we explored whether differences in clinical measurements of overweight participants before and after such intervention could be reflected in their structural brain MRI scans. This was accomplished by exploiting deep learning models for the development of an obesity-related neural biomarker—the brain-BMI gap, and its application to the DIRECT-PLUS clinical trial dataset (Yaskolka Meir et al., 2021). This study is the first of its kind, applying the novel brain-BMI gap biomarker to an obese population which underwent a lifestyle intervention.

The proposed model was based on an ensemble of CNNs, where each was independently trained to predict BMI given a comprehensive dataset of sMRI acquisitions (public dataset). The trained CNN ensemble was then used to predict BMI for the overweight DIRECT-PLUS population. A key difference between the public training dataset and the DIRECT-PLUS datasets was the fact that the BMI distributions of the scanned subjects were different. Specifically, the DIRECT-

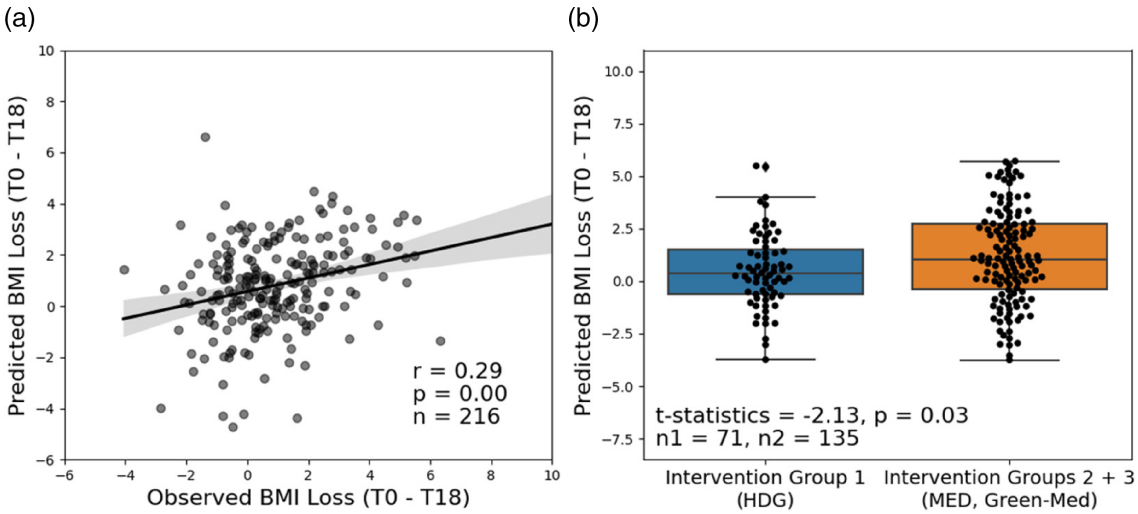


**FIGURE 4** The DIRECT-PLUS dataset. (a) Regression plot showing a significant association between predicted and observed BMI loss, with Pearson correlation coefficient $r = 0.23$ ($p = .00$). (b) Box plot demonstrating the significant difference in predicted BMI loss between intervention groups after bias correction and outliers removal.

**TABLE 2** Location of clusters in the XAI Maps.

| Region | Size | Max value | x | y | z |
|---|---|---|---|---|---|
| Parietal cortex<br>Interhemispheric fissure | 22,904 | 0.579 | −10 | −80 | 51 |
| Interhemispheric fissure<br>Orbitofrontal cortex<br>Anterior cingulate cortex<br>Anterior temporal cortex | 14,763 | 0.753 | 0 | 1 | −32 |
| Lateral occipital cortex<br>Lateral cerebellum | 5200 | 0.606 | 52 | −70 | −17 |
| Right insula | 3175 | 0.497 | 50 | 17 | −7 |
| Interpeduncular cistern | 1981 | 0.538 | 12 | −38 | −9 |
| Left cingulate cortex | 1085 | 0.5 | 1 | 17 | 33 |
| 4th ventricle | 412 | 0.53 | −1 | −44 | −40 |
| Left occipital pole | 351 | 0.468 | −30 | −97 | 5 |
| Right lateral ventricle | 250 | 0.557 | 26 | −44 | 6 |
| Left superior parietal gyrus | 239 | 0.483 | −30 | −45 | 68 |
| Left lateral ventricle | 204 | 0.529 | −21 | −46 | 9 |
| Right cingulate cortex | 145 | 0.486 | −16 | −19 | −32 |
| Right temporal inferior gyrus | 143 | 0.453 | 45 | −17 | −35 |
| Right anterior temporal cortex | 129 | 0.45 | 42 | 6 | −43 |
| Precentral gyrus<br>Superior frontal cortex | 109 | 0.451 | 54 | 15 | 36 |

PLUS population was overweight with high BMI levels. In contrast, our training dataset was of subjects with normal BMI distribution. Additionally, following changes initiated by the lifestyle intervention, the DIRECT-PLUS dataset was highly fluctuative. In addition to the variability of BMIs and weight loss trajectories, we conjecture that there was a possible delay between weight loss and brain morphology. Nevertheless, our model was able to generalize and achieved a BMI prediction error of about 5 units.

We note that there was a reduction in BMI prediction accuracy between the public datasets (Figure 2b) and the DIRECT-PLUS dataset (Figure 2c,d). This may be due to the difference in BMI distribution between the training and the test datasets. It is interesting to note that the prediction error was slightly lower for the DIRECT-PLUS dataset following the intervention (T18). At this time point, the participants' average BMI was reduced, and their BMI distribution was somewhat closer to that of the subjects in the training datasets. This

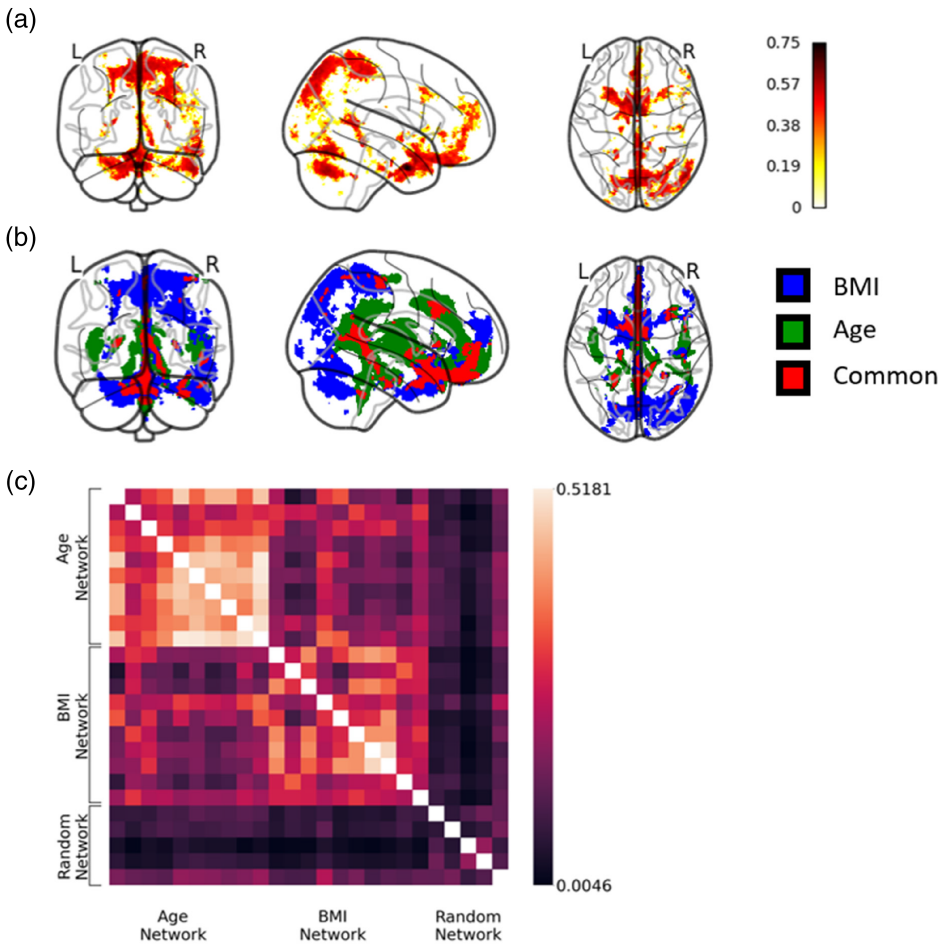


**FIGURE 5** The DIRECT-PLUS dataset ($n = 216$). Regions highlighted by the BMI ensemble model and the differences between age and BMI features at T0. (a) Glass brain projections of the first percentile of the population-based maps of BMI prediction model (b) Glass brain projections depicting the population XAI maps for age (green), BMI (blue) and the regions common for both maps (red). (c) Similarity matrix presenting Dice scores of all possible pairs of population-based explanation maps (before aggregation over separate CNNs, after a threshold of 99%). The color of each of the matrix entries denotes the Dice coefficient between each pair of maps. The Dice scores are color coded between 0 to 1, where higher scores are brighter. As can be seen, there is a higher similarity within group (e.g., BMI and BMI maps) rather than between groups (e.g., age and BMI maps) ($t = 11.663$, $p < .001$).

reduction in test accuracy on an entirely new dataset was also seen in a previous study (Vakli et al., 2020) where BMI distributions were similar. Hence, a more general explanation to the lower test accuracy was a dataset bias (Ashraf et al., 2018; Tommasi et al., 2017; Wachinger et al., 2021).

Despite the MAE obtained for the test dataset, the predicted BMI was still correlated with other obesity-related clinical measures, which validated its clinical relevance and the future potential of the brain-BMI gap biomarker. Importantly, we demonstrated that the predicted BMI was significantly positively correlated with WC, AST, ALT, HOMA-IR, Liver Fat, and VAT and negatively correlated with HDL-C. Furthermore, some of these statistically significant correlations were preserved after controlling for the observed BMI and following FDR correction: HDL-c, liver fat, and VAT. It is worth mentioning that HDL-C is considered a protective type of cholesterol and its deficiency is associated with low GM and WM volume (Wang et al., 2021; Ward et al., 2010) while the high level of visceral fat was associated with lower brain volume (Debette et al., 2010) and reduced cortical thickness (Veit et al., 2014). These results imply that the predicted brain BMI was not only related to observed BMI but also to various other health biomarkers implicated in obesity.

One main advantage of the DIRECT-PLUS trial design was the acquisition of brain imaging both before and after the lifestyle intervention. Statistical analysis of the BMI predictions in the two time points revealed two key findings. First, as shown in Figure 4a, we found a correlation between the actual subject-specific BMI loss and the predicted one. With the absence of available longitudinal data to train on, it was impossible to predict the BMI loss. Therefore, it is based on two separate predictions for T0 and T18 and composed of an accumulated error from both. This may explain the low, yet significant correlation. This result further supports the generalization ability of the proposed brain-BMI prediction model. Second, the plot presented in Figure 4b, which shows the significant prediction difference between the active-control (HDG) and the active-dietary intervention groups (MED, Green-Med), underscores the validity of the brain-BMI biomarker. These findings suggest that the tested forms of lifestyle intervention may result in structural brain changes that can be captured by the proposed biomarker.

A main goal of this research was the identification of the brain regions which contributed to the BMI prediction. For this purpose, we created population-based explanation maps based on the trained CNN ensemble, as presented in Figure 5a and Table 2. Some of the highlighted brain regions include the orbitofrontal cortex, the cerebellum, the right insula, the anterior temporal cortex, and the lateral occipital cortex. We note that XAI maps are not evidence of a direct relation between brain morphology and BMI, which is a tool to

quantify obesity. Hence, we suggest cautiously that the identified regions were related to the manifestation of obesity in the brain. Nevertheless, several previous studies reported such a link between the aforementioned brain regions and excessive weight.

A previous study showed that reduced gray matter volume (GMV) in the orbitofrontal cortex was associated with obese or morbidly obese people (Seabrook & Borgland, 2020) and structural changes in the orbitofrontal cortex were associated with obesity (Chen et al., 2020; Seabrook & Borgland, 2020; Shott et al., 2015). Furthermore, activation of the orbitofrontal cortex was also associated with an eating-related reward system (Seabrook & Borgland, 2020). Reduced GMV was also found in the cerebellum of obese subjects (Pannacciulli et al., 2006), and obesity-related measures were associated with lower GMV in the bilateral cerebellum (García-García et al., 2019). Additionally, a previous study revealed reduced global connectivity in the right insula of adolescents with excess weight compared with normal weight (Moreno-Lopez et al., 2016). Another study revealed that obese patients had reduced GMV in the right insula as well as in the right inferior frontal gyrus (Herrmann et al., 2019). Moreover, an association between BMI and decreased cortical thickness in the insula was found (Veit et al., 2014). Some previous studies also showed that reduced GMV in these regions was associated with increased BMI and increased VAT (Kurth et al., 2013; Medic et al., 2016; Veit et al., 2014). The studies mentioned above provide some supportive evidence to the proposed BMI-related explanation maps, yet the heterogeneity of the methodologies do not allow to draw a direct connection between the highlighted brain regions, BMI and lifestyle intervention.

A previous study used a somewhat similar methodology to predict BMI from T1 MRI scans and analyze regions highlighted by localization maps (Vakli et al., 2020). This study, applied to the UK Biobank and Information eXtraction from Images (IXI) datasets, revealed regions that were mostly different than those found in our study (i.e., the left caudate, the left medial temporal lobe, and the lateral surface of the right temporal cortex). This inconsistency might be explained by the different populations for which the maps were generated, and specifically the difference in the BMI distributions. With no ground truth for comparison, we attempted to validate our results to the best of our ability. First, we utilized an ensemble architecture, which was shown to be robust (Levakov et al., 2020). Second, as discussed above, we confirmed the relationship between obesity and areas revealed by the maps in the literature. Third, we demonstrated the consistency between our maps in Figure 5c. Fourth, to test whether the aforementioned differences can be explained by obesity, we generated maps for obese participants from the UK Biobank dataset and discovered substantial overlap with the brain regions found for the participants in our DIRECT-PLUS study (Data S1, section 6). Although the BMI predictions contained a certain error, the population-based explanation maps were validated and statistically reliable.

Finally, the XAI maps obtained for BMI prediction with those obtained for age prediction for the DIRECT-18 dataset were compared in Figure 5b,c. The minimal overlap between the maps implied that the brain-BMI biomarker was independent of the brain-age biomarker. This is an important result in light of several studies that showed that BMI tends to increase with age (Boutari & Mantzoros, 2022; Chooi et al., 2019; Elia, 2001; Reas et al., 2007).

One of the implications of the DIRECT-PLUS study was the variability in weight-change patterns following the intervention period. For example, two subjects with the same extent of BMI reduction could still have very different weight change trajectories. For some subjects, a significant weight loss was detected about 6 months after the beginning of the intervention but afterward they regained weight (for details, see Figure S3 in Data S1, section 7). This heterogeneity may be reflected in the brain scans conducted in T18. Future work should sample more frequent scanning time points throughout the intervention that would allow us to monitor weight-change dynamics. Dataset bias is a common challenge, particularly where the distributions differ (Tommasi et al., 2017). In our case, the training and testing datasets have different BMI distributions, which affect the predictive performance while testing on higher BMIs. So far, we were not able to locate a publicly available dataset which contains a population with a BMI distribution that matched that of the DIRECT-PLUS's population. Future studies should focus on improving the predictive models, and or train the models on data with more compatible BMI distribution, when available.

## 5 | CONCLUSION

Our findings validate the predicted BMI as a clinically significant neural biomarker. This novel biomarker captures structural changes in the brain that occurred due to weight loss initiated by lifestyle intervention. It is also independent of the brain aging process. To the best of our knowledge, the current study is the first clinical application of the brain-predicted BMI in a randomized control trial. The brain-predicted BMI is a promising, novel framework that allows exploring the link between obesity, weight loss, and the brain.

### ACKNOWLEDGMENTS

We thank Assaf Rudich from Ben-Gurion University and Efrat Puplin, Eyal Goshen, Avi Ben Shabat, and Benjamin Sarusi from the Nuclear Research Center Negev for their valuable contributions. Our project would not have been possible without several open databases and groups that invested considerable resources and efforts to support neuroimaging data sharing. We wish to acknowledge those study groups and funding agencies: ADNI—Data collection and sharing for this project was funded by the Alzheimer's Disease Neuroimaging Initiative (ADNI) (National Institutes of Health Grant U01 AG024904) and DOD ADNI (Department of Defense award number W81XWH-12-2-0012). ADNI is funded by the National Institute on Aging, the National Institute of Biomedical Imaging and Bioengineering, and through generous contributions from the following: AbbVie, Alzheimer's Association; Alzheimer's Drug Discovery Foundation; Araclon Biotech; BioClinica, Inc.; Biogen; BristolMyers Squibb Company; CereSpir, Inc.; Cogstate; Eisai Inc.; Elan Pharmaceuticals, Inc.; Eli Lilly and

Company; EuroImmun; F. Hoffmann-La Roche Ltd and its affiliated company Genentech, Inc.; Fujirebio; GE Healthcare; IXICO Ltd.; Janssen Alzheimer Immunotherapy Research & Development, LLC.; Johnson & Johnson Pharmaceutical Research & Development LLC.; Lumosity; Lundbeck; Merck & Co., Inc.; Meso Scale Diagnostics, LLC.; NeuroRx Research; Neurotrack Technologies; Novartis Pharmaceuticals Corporation; Pfizer Inc.; Piramal Imaging; Servier; Takeda Pharmaceutical Company; and Transition Therapeutics. The Canadian Institutes of Health Research is providing funds to support ADNI clinical sites in Canada. Private sector contributions are facilitated by the Foundation for the National Institutes of Health (www.fnih.org). The grantee organization is the Northern California Institute for Research and Education, and the study is coordinated by the Alzheimer's Therapeutic Research Institute at the University of Southern California. ADNI data are disseminated by the Laboratory for Neuro Imaging at the University of Southern California. ABIDE—Primary support for the work by Adriana Di Martino, and Michael P. Milham and his team was provided by the NIMH (K23MH087770), the Leon Levy Foundation, Joseph P. Healy and the Stavros Niarchos Foundation to the Child Mind Institute, NIMH award to MPM (R03MH096321), National Institute of Mental Health (NIMH 5R21MH107045), Nathan S. Kline Institute of Psychiatric Research), Phyllis Green and Randolph Cowen to the Child Mind Institute. PPMI—Data used in the preparation of this article were obtained from the Parkinson's Progression Markers Initiative (PPMI) database (www.ppmi-info.org/data). For up-to-date information on the study, visit www.ppmi-info.org. PPMI—a public-private partnership—is funded by the Michael J. Fox Foundation for Parkinson's Research and funding partners, including [list of the full names of all of the PPMI funding partners can be found at www.ppmi-info.org/ fundingpartners]. ICBM—Data used in the preparation of this work were obtained from the International Consortium for Brain Mapping (ICBM) database (www.loni.usc.edu/ICBM). The ICBM project (Principal Investigator John Mazziotta, M.D., University of California, Los Angeles) is supported by the National Institute of Biomedical Imaging and BioEngineering. ICBM is the result of efforts of coinvestigators from UCLA, Montreal Neurologic Institute, University of Texas at San Antonio, and the Institute of Medicine, Juelich/Heinrich Heine University—Germany. IXI—Data were provided in part by the IXI database (http://brain-development.org/). CamCan-Data collection and sharing for this project was provided by the Cambridge Centre for Ageing and Neuroscience (CamCAN). CamCAN funding was provided by the UK Biotechnology and Biological Sciences Research Council (grant number BB/H008217/1), together with support from the UK Medical Research Council and University of Cambridge, UK. Data used in the preparation of this work were obtained from the CamCAN repository (available at http://www.mrc-cbu.cam.ac.uk/datasets/camcan/). Uk-Biobank-This research has been conducted using the UK Biobank Resource (www.ukbiobank.ac.uk).

## FUNDING INFORMATION

This work was supported by grants from: the German Research Foundation (DFG), German Research Foundation—project number (209933838-SFB 1052; B11), Israel Ministry of Health grant 87472511 (to Iris Shai); Israel Ministry of Science and Technology grant 3-13604 (to Iris Shai); and the California Walnuts Commission (to Iris Shai).

## CONFLICT OF INTEREST STATEMENT

All authors declare no conflict of interest.

## DATA AVAILABILITY STATEMENT

All the datasets used for the model's training and validation were acquired from open-access data sharing projects. Data from the DIRECT-PLUS trial is not publicly available since it contains information that could compromise the privacy of research participants. However, it could be made available upon request pending approval of Prof. Iris Shai (irish@bgu.ac.il). BMI prediction model code & weights, as well as figures code is available at: https://github.com/ofekfink/BMI_Prediction.git.

## ETHICS STATEMENT

The Soroka Medical Center Medical Ethics Board and Institutional Review Board provided ethics approval.

## ORCID

*Ofek Finkelstein* https://orcid.org/0009-0001-4160-9643
*Galia Avidan* https://orcid.org/0000-0003-2293-3859

## REFERENCES

Adebayo, J., Gilmer, J., Muelly, M., Goodfellow, I., Hardt, M., & Kim, B. (2018). Sanity checks for saliency maps. https://doi.org/10.48550/ARXIV.1810.03292

Alber, M., Lapuschkin, S., Seegerer, P., Hägele, M., Schütt, K. T., Montavon, G., Samek, W., Müller, K.-R., Dähne, S., & Kindermans, P.-J. (2018). iNNvestigate neural networks! https://doi.org/10.48550/ARXIV.1808.04260

Alford, S., Patel, D., Perakakis, N., & Mantzoros, C. S. (2018). Obesity as a risk factor for Alzheimer's disease: Weighing the evidence. *Obesity Reviews*, *19*(2), 269–280. https://doi.org/10.1111/obr.12629

Arjmand, G., Abbas-Zadeh, M., & Eftekhari, M. H. (2022). Effect of MIND diet intervention on cognitive performance and brain structure in healthy obese women: A randomized controlled trial. *Scientific Reports*, *12*(1), 2871. https://doi.org/10.1038/s41598-021-04258-9

Ashraf, A., Khan, S., Bhagwat, N., Chakravarty, M., & Taati, B. (2018). Learning to unlearn: Building immunity to dataset bias in medical imaging studies. https://doi.org/10.48550/ARXIV.1812.01716

Beheshti, I., Nugent, S., Potvin, O., & Duchesne, S. (2019). Bias-adjustment in neuroimaging-based brain age frameworks: A robust scheme. *NeuroImage: Clinical*, *24*, 102063. https://doi.org/10.1016/j.nicl.2019.102063

Benjamini, Y., & Hochberg, Y. (1995). Controlling the false discovery rate: A practical and powerful approach to multiple testing. *Journal of the Royal Statistical Society: Series B (Methodological)*, *57*(1), 289–300. https://doi.org/10.1111/j.2517-6161.1995.tb02031.x

Bocancea, D. I., van Loenhoud, A. C., Groot, C., Barkhof, F., van der Flier, W. M., & Ossenkoppele, R. (2021). Measuring resilience and resistance in aging and Alzheimer disease using residual methods: A systematic review and meta-analysis. *Neurology*, *97*(10), 474–488. https://doi.org/10.1212/WNL.0000000000012499

Boutari, C., & Mantzoros, C. S. (2022). A 2022 update on the epidemiology of obesity and a call to action: As its twin COVID-19 pandemic appears to be receding, the obesity and dysmetabolism pandemic continues to rage on. *Metabolism*, *133*, 155217. https://doi.org/10.1016/j.metabol.2022.155217

Chen, E. Y., Eickhoff, S. B., Giovannetti, T., & Smith, D. V. (2020). Obesity is associated with reduced orbitofrontal cortex volume: A coordinate-based meta-analysis. *NeuroImage: Clinical*, *28*, 102420. https://doi.org/10.1016/j.nicl.2020.102420

Chollet, F. (2018). Keras: The python deep learning library. Astrophysics source code library, ascl-180.022.

Chooi, Y. C., Ding, C., & Magkos, F. (2019). The epidemiology of obesity. *Metabolism*, *92*, 6–10. https://doi.org/10.1016/j.metabol.2018.09.005

Cole, J. H., Poudel, R. P. K., Tsagkrasoulis, D., Caan, M. W. A., Steves, C., Spector, T. D., & Montana, G. (2017). Predicting brain age with deep learning from raw imaging data results in a reliable and heritable biomarker. *NeuroImage*, *163*, 115–124. https://doi.org/10.1016/j.neuroimage.2017.07.059

Cole, J. H., Ritchie, S. J., Bastin, M. E., Valdés Hernández, M. C., Muñoz Maniega, S., Royle, N., Corley, J., Pattie, A., Harris, S. E., Zhang, Q., Wray, N. R., Redmond, P., Marioni, R. E., Starr, J. M., Cox, S. R., Wardlaw, J. M., Sharp, D. J., & Deary, I. J. (2018). Brain age predicts mortality. *Molecular Psychiatry*, *23*(5), 1385–1392. https://doi.org/10.1038/mp.2017.62

Debette, S., Beiser, A., Hoffmann, U., DeCarli, C., O'Donnell, C. J., Massaro, J. M., Au, R., Himali, J. J., Wolf, P. A., Fox, C. S., & Seshadri, S. (2010). Visceral fat is associated with lower brain volume in healthy middle-aged adults. *Annals of Neurology*, *68*, 136–144. https://doi.org/10.1002/ana.22062

Desikan, R. S., Ségonne, F., Fischl, B., Quinn, B. T., Dickerson, B. C., Blacker, D., Buckner, R. L., Dale, A. M., Maguire, R. P., Hyman, B. T., Albert, M. S., & Killiany, R. J. (2006). An automated labeling system for subdividing the human cerebral cortex on MRI scans into gyral based regions of interest. *NeuroImage*, *31*(3), 968–980. https://doi.org/10.1016/j.neuroimage.2006.01.021

Dice, L. R. (1945). Measures of the amount of ecologic association between species. *Ecology*, *26*(3), 297–302. https://doi.org/10.2307/1932409

Elia, M. (2001). Obesity in the elderly. *Obesity Research*, *9*(S11), 244S–248S. https://doi.org/10.1038/oby.2001.126

Espeland, M. A., Erickson, K., Neiberg, R. H., Jakicic, J. M., Wadden, T. A., Wing, R. R., Desiderio, L., Erus, G., Hsieh, M.-K., Davatzikos, C., Maschak-Carey, B. J., Laurienti, P. J., Demos-McDermott, K., Bryan, R. N., & for the Action for Health in Diabetes Brain Magnetic Resonance Imaging (Look AHEAD Brain) Ancillary Study Research Group. (2016). Brain and white matter hyperintensity volumes after 10 years of random assignment to lifestyle intervention. *Diabetes Care*, *39*(5), 764–771. https://doi.org/10.2337/dc15-2230

Fischl, B. (2012). FreeSurfer. *NeuroImage*, *62*(2), 774–781. https://doi.org/10.1016/j.neuroimage.2012.01.021

Franke, K., Luders, E., May, A., Wilke, M., & Gaser, C. (2012). Brain maturation: Predicting individual BrainAGE in children and adolescents using structural MRI. *NeuroImage*, *63*(3), 1305–1312. https://doi.org/10.1016/j.neuroimage.2012.08.001

García-García, I., Michaud, A., Dadar, M., Zeighami, Y., Neseliler, S., Collins, D. L., Evans, A. C., & Dagher, A. (2019). Neuroanatomical differences in obesity: Meta-analytic findings and their validation in an independent dataset. *International Journal of Obesity*, *43*(5), 943–951. https://doi.org/10.1038/s41366-018-0164-4

Gierach, M., Gierach, J., Ewertowska, M., Arndt, A., & Junik, R. (2014). Correlation between body mass index and waist circumference in patients with metabolic syndrome. *ISRN Endocrinology*, *2014*, 514589. https://doi.org/10.1155/2014/514589

Gorgolewski, K., Burns, C., Madison, C., Clark, D., Halchenko, Y., Waskom, M., & Ghosh, S. (2011). Nipype: A flexible, lightweight and extensible neuroimaging data processing framework in python. *Frontiers in Neuroinformatics*, *5*. https://doi.org/10.3389/fninf.2011.00013

Han, Y.-P., Tang, X., Han, M., Yang, J., Cardoso, M. A., Zhou, J., & Simó, R. (2021). Relationship between obesity and structural brain abnormality: Accumulated evidence from observational studies. *Ageing Research Reviews*, *71*, 101445. https://doi.org/10.1016/j.arr.2021.101445

Herrmann, M. J., Tesar, A., Beier, J., Berg, M., & Warrings, B. (2019). Grey matter alterations in obesity: A meta-analysis of whole-brain studies. *Obesity Reviews*, *20*(3), 464–471. https://doi.org/10.1111/obr.12799

Iglesias, J. E., Liu, C.-Y., Thompson, P. M., & Tu, Z. (2011). Robust brain extraction across datasets and comparison with publicly available methods. *IEEE Transactions on Medical Imaging*, *30*(9), 1617–1634. https://doi.org/10.1109/TMI.2011.2138152

Jenkinson, M., Beckmann, C. F., Behrens, T. E. J., Woolrich, M. W., & Smith, S. M. (2012). FSL. *NeuroImage*, *62*(2), 782–790. https://doi.org/10.1016/j.neuroimage.2011.09.015

Kaplan, A., Zelicha, H., Yaskolka Meir, A., Rinott, E., Tsaban, G., Levakov, G., Prager, O., Salti, M., Yovell, Y., Ofer, J., Huhn, S., Beyer, F., Witte, V., Villringer, A., Meiran, N., Emesh, B. T., Kovacs, P., Von Bergen, M., Ceglarek, U., … Shai, I. (2022). The effect of a high-polyphenol Mediterranean diet (green-MED) combined with physical activity on age-related brain atrophy: The dietary intervention randomized controlled trial polyphenols Unprocessed study (DIRECT PLUS). *The American Journal of Clinical Nutrition*, *115*(5), 1270–1281. https://doi.org/10.1093/ajcn/nqac001

Kivipelto, M., Ngandu, T., Fratiglioni, L., Viitanen, M., Kåreholt, I., Winblad, B., Helkala, E.-L., Tuomilehto, J., Soininen, H., & Nissinen, A. (2005). Obesity and vascular risk factors at midlife and the risk of dementia and Alzheimer disease. *Archives of Neurology*, *62*(10), 1556–1560. https://doi.org/10.1001/archneur.62.10.1556

Kurth, F., Levitt, J. G., Phillips, O. R., Luders, E., Woods, R. P., Mazziotta, J. C., Toga, A. W., & Narr, K. L. (2013). Relationships between gray matter, body mass index, and waist circumference in healthy adults. *Human Brain Mapping*, *34*(7), 1737–1746. https://doi.org/10.1002/hbm.22021

Leong, K. S., & Wilding, J. P. (1999). Obesity and diabetes. *Best Practice & Research Clinical Endocrinology & Metabolism*, *13*(2), 221–237. https://doi.org/10.1053/beem.1999.0017

Levakov, G., Kaplan, A., Yaskolka Meir, A., Rinott, E., Tsaban, G., Zelicha, H., Bluher, M., Ceglarek, U., Stumvoll, M., Shelef, I., Avidan, G., & Shai, I. (2023). The effect of weight loss following 18 months of lifestyle intervention on brain age assessed with resting-state functional connectivity. *ELife*, 12, e83604. https://doi.org/10.7554/elife.83604

Levakov, G., Rosenthal, G., Shelef, I., Raviv, T. R., & Avidan, G. (2020). From a deep learning model back to the brain-identifying regional predictors and their relation to aging. *Human Brain Mapping*, *41*(12), 3235–3252. https://doi.org/10.1002/hbm.25011

Lund, M. J., Alnæs, D., de Lange, A.-M. G., Andreassen, O. A., Westlye, L. T., & Kaufmann, T. (2022). Brain age prediction using fMRI network coupling in youths and associations with psychiatric symptoms. *NeuroImage: Clinical*, *33*, 102921. https://doi.org/10.1016/j.nicl.2021.102921

Medic, N., Ziauddeen, H., Ersche, K. D., Farooqi, I. S., Bullmore, E. T., Nathan, P. J., Ronan, L., & Fletcher, P. C. (2016). Increased body mass index is associated with specific regional alterations in brain structure. *International Journal of Obesity*, *40*(7), 1177–1182. https://doi.org/10.1038/ijo.2016.42

Moreno-Lopez, L., Contreras-Rodriguez, O., Soriano-Mas, C., Stamatakis, E. A., & Verdejo-Garcia, A. (2016). Disrupted functional connectivity in adolescent obesity. *NeuroImage: Clinical*, *12*, 262–268. https://doi.org/10.1016/j.nicl.2016.07.005

Mori, S., Wakana, S., van Zijl, P. C. M., & Nagae-Poetscher, L. M. (2006). MRI atlas of human white matter. *AJNR: American Journal of Neuroradiology*, *27*(6), 1384–1385.

Nguyen, J. C. D., Killcross, A. S., & Jenkins, T. A. (2014). Obesity and cognitive decline: Role of inflammation and vascular changes. *Frontiers in Neuroscience*, *8*, 375. https://doi.org/10.3389/fnins.2014.00375

Pannacciulli, N., Del Parigi, A., Chen, K., Le, D. S. N. T., Reiman, E. M., & Tataranni, P. A. (2006). Brain abnormalities in human obesity: A voxel-

based morphometric study. *NeuroImage*, *31*(4), 1419–1425. https://doi.org/10.1016/j.neuroimage.2006.01.047

Razay, G., Vreugdenhil, A., & Wilcock, G. (2006). Obesity, abdominal obesity and Alzheimer disease. *Dementia and Geriatric Cognitive Disorders*, *22*(2), 173–176. https://doi.org/10.1159/000094586

Reas, D. L., Nygård, J. F., Svensson, E., Sørensen, T., & Sandanger, I. (2007). Changes in body mass index by age, gender, and socio-economic status among a cohort of Norwegian men and women (1990–2001). *BMC Public Health*, *7*(1), 269. https://doi.org/10.1186/1471-2458-7-269

Reinhold, J. C., Dewey, B. E., Carass, A., & Prince, J. L. (2018). Evaluating the impact of intensity normalization on MR image synthesis. https://doi.org/10.48550/ARXIV.1812.04652

Scheen, A. J., & Luyckx, F. H. (2002). Obesity and liver disease. *Best Practice & Research Clinical Endocrinology & Metabolism*, *16*(4), 703–716. https://doi.org/10.1053/beem.2002.0225

Seabrook, L. T., & Borgland, S. L. (2020). The orbitofrontal cortex, food intake and obesity. *Journal of Psychiatry and Neuroscience*, *45*(5), 304–312. https://doi.org/10.1503/jpn.190163

Shefer, G., Marcus, Y., & Stern, N. (2013). Is obesity a brain disease? *Neuroscience & Biobehavioral Reviews*, *37*(10), 2489–2503. https://doi.org/10.1016/j.neubiorev.2013.07.015

Shott, M. E., Cornier, M.-A., Mittal, V. A., Pryor, T. L., Orr, J. M., Brown, M. S., & Frank, G. K. W. (2015). Orbitofrontal cortex volume and brain reward response in obesity. *International Journal of Obesity (2005)*, *39*(2), 214–221. https://doi.org/10.1038/ijo.2014.121

Smilkov, D., Thorat, N., Kim, B., Viégas, F., & Wattenberg, M. (2017). SmoothGrad: Removing noise by adding noise. https://doi.org/10.48550/ARXIV.1706.03825

Spyridaki, E. C., Avgoustinaki, P. D., & Margioris, A. N. (2016). Obesity, inflammation and cognition. *Current Opinion in Behavioral Sciences*, *9*, 169–175. https://doi.org/10.1016/j.cobeha.2016.05.004

Student. (1908). The probable error of a mean. *Biometrika*, *6*(1), 1. https://doi.org/10.2307/2331554

Tommasi, T., Patricia, N., Caputo, B., & Tuytelaars, T. (2017). A deeper look at dataset bias. In G. Csurka (Ed.), *Domain adaptation in computer vision applications* (pp. 37–55). Springer International Publishing. https://doi.org/10.1007/978-3-319-58347-1_2

Tustison, N. J., Avants, B. B., Cook, P. A., Zheng, Y., Egan, A., Yushkevich, P. A., & Gee, J. C. (2010). N4ITK: Improved N3 bias correction. *IEEE Transactions on Medical Imaging*, *29*(6), 1310–1320. https://doi.org/10.1109/TMI.2010.2046908

Uranga, R. M., & Keller, J. N. (2019). The complex interactions between obesity, metabolism and the brain. *Frontiers in Neuroscience*, *13*, 513. https://doi.org/10.3389/fnins.2019.00513

Vakli, P., Deák-Meszlényi, R. J., Auer, T., & Vidnyánszky, Z. (2020). Predicting body mass index from structural MRI brain images using a deep convolutional neural network. *Frontiers in Neuroinformatics*, *14*, 10. https://doi.org/10.3389/fninf.2020.00010

van der Walt, S., Schönberger, J. L., Nunez-Iglesias, J., Boulogne, F., Warner, J. D., Yager, N., Gouillart, E., Yu, T., & Scikit-Image Contributors. (2014). scikit-image: Image processing in python. *PeerJ*, *2*, e453. https://doi.org/10.7717/peerj.453

Veit, R., Kullmann, S., Heni, M., Machann, J., Häring, H.-U., Fritsche, A., & Preissl, H. (2014). Reduced cortical thickness associated with visceral fat and BMI. *NeuroImage: Clinical*, *6*, 307–311. https://doi.org/10.1016/j.nicl.2014.09.013

Wachinger, C., Rieckmann, A., & Pölsterl, S. (2021). Detect and correct bias in multi-site neuroimaging datasets. *Medical Image Analysis*, *67*, 101879. https://doi.org/10.1016/j.media.2020.101879

Wang, M., Li, Y., Cong, L., Hou, T., Luo, Y., Shi, L., Chang, L., Zhang, C., Wang, Y., Wang, X., Du, Y., & Qiu, C. (2021). High-density lipoprotein cholesterol and brain aging amongst rural-dwelling older adults: A population-based magnetic resonance imaging study. *European Journal of Neurology*, *28*(9), 2882–2892. https://doi.org/10.1111/ene.14939

Ward, M. A., Bendlin, B. B., Mclaren, D. G., Hess, T. M., Gallagher, C. L., Kastman, E. K., Rowley, H. A., Asthana, S., Carlsson, C. M., Sager, M. A., & Johnson, S. C. (2010). Low HDL cholesterol is associated with lower gray matter volume in cognitively healthy adults. *Frontiers in Aging Neuroscience.*, *2*, 29. https://doi.org/10.3389/fnagi.2010.00029

Weiss, R., Dziura, J., Burgert, T. S., Tamborlane, W. V., Taksali, S. E., Yeckel, C. W., Allen, K., Lopes, M., Savoye, M., Morrison, J., Sherwin, R. S., & Caprio, S. (2004). Obesity and the metabolic syndrome in children and adolescents. *New England Journal of Medicine*, *350*(23), 2362–2374. https://doi.org/10.1056/NEJMoa031049

Whitmer, R. A., Gunderson, E. P., Barrett-Connor, E., Quesenberry, C. P., & Yaffe, K. (2005). Obesity in middle age and future risk of dementia: A 27 year longitudinal population based study. *BMJ*, *330*(7504), 1360. https://doi.org/10.1136/bmj.38446.466238.E0

Woolrich, M. W., Jbabdi, S., Patenaude, B., Chappell, M., Makni, S., Behrens, T., Beckmann, C., Jenkinson, M., & Smith, S. M. (2009). Bayesian analysis of neuroimaging data in FSL. *NeuroImage*, *45*(1), S173–S186. https://doi.org/10.1016/j.neuroimage.2008.10.055

Yadav, C., & Razavian, N. (2019). Using brain MRI images to predict memory, BMI & age. *2019 IEEE International Conference on Humanized Computing and Communication*, 126–128. https://doi.org/10.1109/HCC46620.2019.00026

Yaskolka Meir, A., Rinott, E., Tsaban, G., Zelicha, H., Kaplan, A., Rosen, P., Shelef, I., Youngster, I., Shalev, A., Blüher, M., Ceglarek, U., Stumvoll, M., Tuohy, K., Diotallevi, C., Vrhovsek, U., Hu, F., Stampfer, M., & Shai, I. (2021). Effect of green-Mediterranean diet on intrahepatic fat: The DIRECT PLUS randomised controlled trial. *Gut*, *70*(11), 2085–2095. https://doi.org/10.1136/gutjnl-2020-323106

## SUPPORTING INFORMATION

Additional supporting information can be found online in the Supporting Information section at the end of this article.

**How to cite this article:** Finkelstein, O., Levakov, G., Kaplan, A., Zelicha, H., Meir, A. Y., Rinott, E., Tsaban, G., Witte, A. V., Blüher, M., Stumvoll, M., Shelef, I., Shai, I., Riklin Raviv, T., & Avidan, G. (2024). Deep learning-based BMI inference from structural brain MRI reflects brain alterations following lifestyle intervention. *Human Brain Mapping*, *45*(3), e26595. https://doi.org/10.1002/hbm.26595